Werk

Terms and Conditions

Contact

Niedersächsische Staats- und Universitätsbibliothek Göttingen
Georg-August-Universität Göttingen
Platz der Göttinger Sieben 1
37073 Göttingen
Germany
Email: gdz@sub.uni-goettingen.de

J. Geophys. 43, 3–31, 1977

Journal of Geophysics

Full Wave Theory Applied to a Discontinuous Velocity Increase: The Inner Core Boundary *

V.F. Cormier [1, 2] and P.G. Richards [1]

Lamont-Doherty Geological Observatory of Columbia University, Palisades, N. Y. 10964, USA

Abstract. Recent developments in the computation of theoretical seismograms have shown the advantages of numerical integrations in the complex ray parameter plane. We here extend the approach, to calculate the amplitude of body waves interacting with a discontinuous velocity increase. The method incorporates a complex velocity profile to account for attenuation and the uniformly asymptotic method of Langer to account for frequency-dependence of reflection-transmission coefficients near grazing incidence. In the integrand of reflection-transmission coefficients, the Debye ray expansion is not made where it is poorly convergent near critical incidence. The method thereby correctly evaluates all the waves in the high velocity medium that are repeatedly refracted back up to, and reflected from, the low velocity medium. Calculations are equally efficient both for earth models specified on discrete radii or as analytic functions of radius.

The method is used to calculate theoretical seismograms for PKP waves in the PEM earth model in the distance range 110°–152° and in earth models 1066B and C2 in the distance range 112°–132°. Calculations of the amplitude near point *D* of the travel time curve for PKP (which is the critical distance of *K* waves incident from the fluid core upon the solid inner core) indicate that at finite frequencies the amplitude maximum associated with critical incidence is smaller than that that would be inferred from frequency independent reflection-transmission coefficients. At lower frequencies the maximum is displaced to a longer distance than *D*. Comparison of observed and calculated seismograms indicates that the PEM model having a *P* velocity jump of 0.83 km/s at the inner core can fit the observed amplitudes.

* Lamont-Doherty Geological Observatory Contribution Number 2500

1 Also Department of Geological Sciences, Columbia University

2 Now at CIRES, University of Colorado, Boulder, Col. 80302

Consequently the data do not require an anomalous P velocity gradient at the top of the inner core. A low frequency precursor to the DF branch of PKP at distances shorter than the B caustic at 146° agrees with Buchbinder's (1974) explanation of diffraction from the B caustic.

Key words: Theoretical seismograms – Earth's core – Interference head wave.

Introduction

Theoretical seismograms enable the amplitude and waveform of body waves to be incorporated as constraints in an inversion scheme for an earth model. Theoretical seismograms can be generated by a variety of methods. Helmberger (1968) described how calculation of theoretical seismograms directly in the time domain by the Cagniard-de Hoop method can be applied to multilayered flat earth models. Gilbert and Helmberger (1972) generalized the Cagniard method to a layered sphere. Other methods seek to evaluate an integral representation of the Fourier-transformed seismogram. This integral representation follows from either the Watson transform or Poisson sum formula for the partial wave series. Its application to the calculation of the amplitudes of seismic body waves in the Earth was first described by Scholte (1956).

In seismic, as well as in general problems of wave scattering, this representation is usually taken to be an integral over wavenumber. Phinney and Alexander (1966) discussed the evaluation of the order number integral for a P wave diffracted by the earth's core. Fuchs and Müller's (1971) reflectivity method converts the integral over horizontal wavenumber to one over real angles of incidence. Richards (1973) demonstrated the computational advantages of taking the representation to be an integral over ray parameter along a path in the complex ray parameter plane. For seismic applications, this modification simply amounts to factoring out frequency from the order number ν (i.e. horizontal wavenumber, or angular wavenumber) using the relation

$$\nu = \omega p - \tfrac{1}{2} \tag{1}$$

where ν is order number, p ray parameter in s/rad and ω radian-frequency. (The term $-\frac{1}{2}$ here corrects for a polar phase shift.)

Richards (1973) applied his method in the frequency domain, incorporating frequency dependence of reflection-transmission coefficients, to calculate the amplitudes of the multiple PmKP waves that result from a P wave grazing the discontinuous P velocity decrease at the core-mantle boundary. Choy (1977) demonstrated that Richards' method allows an inexpensive calculation of theoretical seismograms after Fourier inversion in the time domain.

This paper will report on an extension of the method to the problem of a discontinuous velocity increase, obtaining results which are valid at both grazing and critical incidence. As an example, the method will be applied to calculation of theoretical seismograms for PKP interacting with the discontinuous P velocity increase at the inner core-outer core boundary.

Basic Method

Integral Representation of Displacement

From Richards (1973) the Fourier transformed displacement u at a distance Δ_0 and radian frequency ω is given by

$$u(\Delta_0, \omega) = \int_\Gamma \omega^{\frac{1}{2}} f(p, \Delta_0)\, e^{i\omega J(p, \Delta_0)}\, dp, \tag{2}$$

where Γ is a path in the complex ray parameter (p) plane; $f(p, \Delta_0)$ is a product of reflection-transmission coefficients and the source-receiver directivity function; and $J(p, \Delta_0)$ is the phase delay factor.

The phase delay factor is related to the travel time and distance integrals by

$$J(p, \Delta_0) = T(p) - p\Delta(p) + p\Delta_0. \tag{3}$$

More specifically the phase delay factor is given by

$$J(p, \Delta_0) = \int_{r_p}^{r_s} [1/\alpha^2(r) - p^2/r^2]^{\frac{1}{2}}\, dr + \int_{r_p}^{r_0} [1/\alpha^2(r) - p^2/r^2]^{\frac{1}{2}}\, dr + p\Delta_0 \tag{4}$$

where r_0 is the radius of the receiver, r_s the radius at the source, r_p the radius at which the integrand vanishes, and the integrand is related to the cosine of the angle of incidence by:

$$[1/\alpha^2(r) - p^2/r^2]^{\frac{1}{2}} = \cos i/\alpha(r). \tag{5}$$

Thus the radius r_p is the turning point radius, that radius where the ray bottoms and $\cos i = 0$.

Solution in the Time Domain

Taking the inverse Fourier transform of Equation (2) results in

$$u(\Delta_0, t) = \frac{1}{\pi} \int_0^\infty \omega^{\frac{1}{2}} \operatorname{Re}\left\{\int_\Gamma f e^{i\omega J}\, dp\, e^{-i\omega t}\right\} d\omega. \tag{6}$$

Some methods obtain a solution in the time domain by directly operating with Equation (6). The Cagniard method for a sphere (Gilbert and Helmberger, 1972) achieves this by operating with Equation (6) in terms of Laplace transforms, in which $-i\omega \to s$, and choosing the path in the complex ray parameter plane to be exactly a path of stationary phase. Chapman (1976) described how the solution in the time domain can also be obtained by the first motion approximation, which evaluates the double integral in Equation (6) by the equal phase method.

Richards (1973) enumerated the advantages that accrue to the more general procedure of solving Equation (2) in the frequency domain by a numerical integration along a path Γ in the complex ray parameter plane and then

obtaining the time domain solution by inverse Fourier transformation. In review, these advantages are (i) that, unlike the Cagniard method, the path Γ may remain fixed for a series of distances, the only constraints being that Γ be sufficiently near all ray theory saddles and end in regions in which the integrand is exponentially small; (ii) that the method can be extended for ray paths having a turning point; (iii) that the path Γ automatically includes the non-ray theoretical effects of diffraction given by the residue contribution of ray parameter poles in the reflection-transmission coefficients; and (iv) that effects of attenuation are easily incorporated by allowing the velocity profile to be complex.

Frequency Dependence of Reflection-Transmission Coefficients

Advantages (ii) and (iii) permit a physical description of such phenomena as caustics and diffraction and the frequency dependence of reflection-transmission coefficients. For a body wave incident on a first order velocity discontinuity these coefficients depend significantly on frequency whenever the discontinuity surface is curved or whenever the medium on one or both sides of the discontinuity is radially inhomogeneous.

Alternative methods of calculating theoretical seismograms, such as the Cagniard method or reflectivity method, account for this frequency dependence by the interference properties of multiple reflections in a stack of homogeneous planar layers near the discontinuity. All the multiples are retained in the reflectivity method, whereas the Cagniard method is restricted in practice to retaining a finite (usually small) subset.

In contrast to methods that model radial inhomogeneity by stacks of homogeneous layers, the method used in this paper allows that inhomogeneity to be modeled by functions that are analytic over large ranges of depth. The method thereby minimizes the number of discontinuities required to describe the radial inhomogeneity of the Earth.

In this method, the frequency dependence of reflection-transmission coefficients follows from properties of the exact radial eigenfunctions near the turning point of a ray. WKBJ approximations fail in this region. Consequently the frequency independent reflection-transmission coefficients, which would be given by the WKBJ approximation, are inaccurate near grazing incidence. By applying Langer's (1949) uniformly asymptotic approximation to the radial eigenfunctions, Richards (1976) obtained multiplicative correction factors to the plane wave cosines. Substitution of these Langer corrected cosines makes the reflection-transmission coefficients uniformly valid for all ray parameters both near and far from grazing incidence. This powerful property follows from the ability of the Langer approximation to automatically reproduce the WKBJ and Airy approximations when appropriate. Thus, the Langer approximation automatically corrects for dependence on frequency, radius of curvature of the discontinuity, and Earth structure near the discontinuity.

The appendix of this paper illustrates the details of the Langer approximation applied to the reflection-transmission coefficients for a compressional wave

incident on the inner core boundary. Figures A1 to A3 in the appendix and the calculations by Richards (1976) show that frequency dependence becomes more important over a wider range of angular incidence near grazing as the period of the wave increases. This effect is therefore especially important to include in the calculation of long period synthetic seismograms.

Representation for P Waves Radiated by an Explosive Point Source

For this case the Fourier transformed radial displacement is given by Richards (1973) as

$$u_r(r_s, \Delta_0, \omega) = \frac{F e^{i\pi/4}}{4\pi\rho_s \alpha_s^2 r_s^2} \left(\frac{\omega}{2\pi \sin \Delta_0}\right)^{\frac{1}{2}} \int_\Gamma p^{\frac{1}{2}} f(p, \omega)\, e^{i\omega[J(p, \Delta_0)]}\, dp \tag{7}$$

where source and receiver radii are equal and the source is a body force given by the gradient of potential $F\delta(\mathbf{r}-\mathbf{r}_s)H(t)$.

ρ_s = density at the source depth;
α_s = P velocity at source depth;
r_s = radius at source depth;
$f(p, \omega)$ = product of reflection-transmission and phase conversion coefficients.

This integral reduces trivially to ray theory and the geometrical spreading formula if it is assumed that the only contribution to the integral occurs at discrete saddle points along the real ray parameter axis and that $f(p, \omega)$ is given accurately by the frequency independent plane wave reflection-transmission coefficients. By abandoning these assumptions and numerically integrating along a path Γ, this study will include important non-ray theoretical effects.

Calculations in an Earth Model

The parameter ξ needed in the Langer approximation (Appendix) and the integral quantities in the phase delay factor J can be evaluated by standard ray theory programs that evaluate T and Δ as a function of ray parameter. See, for example, Julian and Anderson (1968). For an earth model specified on discrete radii one can assume the Mohovoričić interpolation law for velocity, yielding a velocity profile of the type

$$\alpha(r) = a_i r^{b_i},\ r_i \leqq r \leqq r_{i+n}, \qquad i = 1, \ldots, N \tag{8}$$

where a_i and b_i are constants calculated from the velocity specified on N radii. Substitution of Equation (8) in Equations (A5) and (4) makes ξ and J equal to linear combinations of transcendental functions. ξ and J, however, can be computed just as effectively in earth models in which the velocity profile is specified by functions that are analytic over large ranges of depth. Dziewonski et al. (1975) demonstrated how such earth models may be constructed as poly-

nomials in radius of order three or less. For these earth models the integrals for ξ and J can be found by quadrature after a numerical calculation of the turning point radius r_p appropriate to a given ray parameter (Cormier, 1976).

Application to a Discontinuous Velocity Increase

$T-\Delta$ Curve and Ray Paths

Common to all discontinuous or rapid increases of velocity in the earth is a triplication in the travel time curve. The velocity increase at the inner core boundary produces the triplication CDF in the $T-\Delta$ curve for PKP (Fig. 1).

The branch CD represents a phase PKiKP totally reflected from the top of the inner core. The continuation of this branch to distances shorter than point D (dashed in Fig. 1) marks the arrival of a partially reflected PKiKP phase. The phase PKIKP transmitted through the inner core is given by the DF branch. For a velocity increase the distance range greater than D can also be termed the lit or total reflection zone and the distance range less than D the shadow or partial reflection zone (Nussenzveig, 1969; Ludwig, 1970). Point D, the critical point, corresponds to grazing incidence on the lower side of the boundary in the higher velocity medium and point C to grazing incidence on the upper side of the boundary in the lower velocity medium.

At distances greater than D, in addition to the singly transmitted DF branch, there exist an infinite number of branches representing rays that are multiply reflected from the underside of the boundary. The dotted line in Figure 1 represents the composite branch of the infinite sum of these interfering multiples. The singly transmitted phase PKIKP shown by the solid line DF cannot be identified as an arrival separate from the interfering sum until beyond 135°. The singly reflected multiple PKIIKP does not separate from the interfering sum until 150°. The composite branch of interfering multiples has been termed an *interference head wave* by Červený (1971). An interference head wave exists for a discontinuous velocity increase when the lower (faster) velocity medium has a positive velocity gradient with depth or when the discontinuity surface is concave downward. Figure 2 gives an example of the ray paths of some of the multiples composing an interference head wave. Because the energy lost upon each of these internal reflections is small for finite frequencies near critical incidence, many of these multiples must be summed for the total amplitude near the PKP-D cusp.

Extension of Method near Critical Incidence

Rather than truncating this sum of multiples after a finite number of terms, it is possible by proper choice of the function f and the path Γ in Equation (7) to include the effect of the infinite sum near critical incidence and to properly evaluate the interference head wave. Earlier studies in full wave theory near critical incidence differ primarily in the choices for Γ and f. Those by

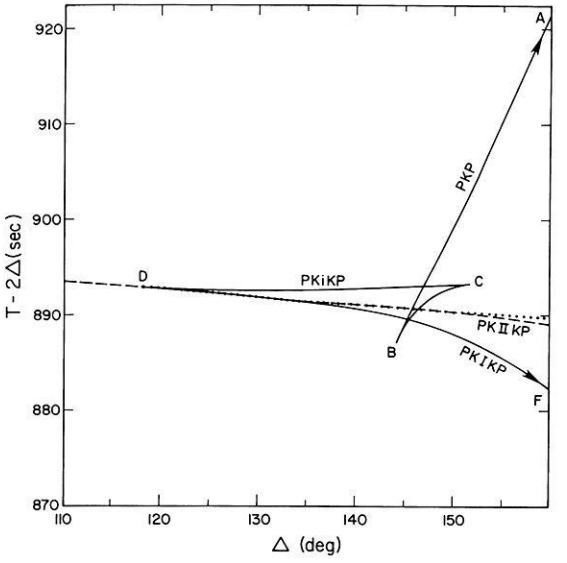

Fig. 1. Reduced travel time curve for PKP in earth model 1066B. Weaker arrivals dashed are the partial reflection PKiKP at distances less than D and PKIIKP once reflected at the underside of the inner core boundary at distances greater than 150 degrees. Interference head wave along the inner core boundary is dotted

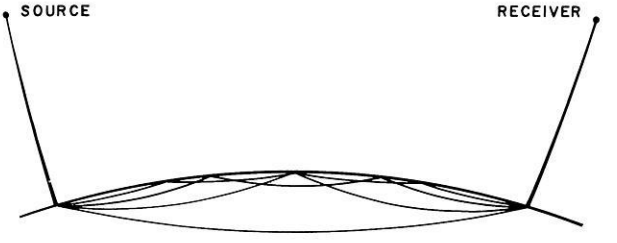

Fig. 2. Examples of multiple internal reflections composing the interference head wave near critical incidence. Shown are the simple transmitted and the rays reflected one, two, and three times from the underside of the boundary in the medium of higher velocity

Nussenzveig (1969) and Ludwig (1970) each make different predictions regarding the diffracted rays and the nature of the transition from the region of partial to total reflection.

The integrand and path decomposition we chose are similar to those proposed by Ludwig (1970). For PKP in the distance range 110°–152°, the product of reflection-transmission coefficients in the integrand of Equation (7) is taken to be

$$f(p,\omega)=\left[T_{PK}^{\downarrow}\frac{m^{(2)}_{\omega p-\frac{1}{2}}(r_m)}{k^{(2)}_{\omega p-\frac{1}{2}}(r_m)}\right] S_I \left[T_{KP}^{\uparrow}\frac{k^{(1)}_{\omega p-\frac{1}{2}}(r_m)}{m^{(1)}_{\omega p-\frac{1}{2}}(r_m)}\right] \tag{9}$$

where $T_{PK}^{\downarrow}$ and $T_{KP}^{\uparrow}$ are the transmission coefficients for a P wave incident on the core-mantle boundary from the mantle and outer core sides respectively. $m_{\omega p-\frac{1}{2}}^{(1)(2)}$ and $k_{\omega p-\frac{1}{2}}^{(1)(2)}$ are radial eigenfunctions in the mantle and outer core respectively, evaluated at the radius r_m of the core-mantle boundary. The superscript (1) refers to an upgoing wave and (2) to a downgoing wave. The function S_I is determined from the boundary condition at the inner core-outer core boundary, allowing for both up and downgoing waves on both sides of the boundary.

Substitution of Equation (9) in Equation (7) requires that the mantle velocity profile be used for the calculation of the phase factor J. For ray parameters bottoming at a radius below the core-mantle boundary, J is calculated in a pseudo velocity profile defined by the downward extrapolation of the mantle velocity profile. Depending on the earth model, this extrapolation is given either by the Mohovoričić velocity function in the lowermost mantle layer or by an analytic velocity function for the lower mantle.

Because J is calculated in the mantle velocity profile, a correction to J is necessary to account properly for the phase accumulated along the K leg of the ray path in the outer core. This correction is accomplished by the ratios of the radial eigenfunctions appearing in Equation (9) and multiplying the coefficients $T_{PK}^{\downarrow}$ and $T_{KP}^{\uparrow}$. Such ratios arise naturally whenever a boundary condition is formulated in terms of radial eigenfunctions (Scholte, 1956).

For a real ray parameter corresponding to a ray bottoming in the outer core and in the limit of $\omega \to \infty$, $S_I \to 1$; the coefficients $T_{PK}^{\downarrow}$ and $T_{KP}^{\uparrow}$ may be replaced by plane wave formulae; and the ratios of the radial eigenfunctions incorporated into the phase factor J. In this case J is calculated by assuming the mantle velocity profile above and the outer core velocity profile below the core-mantle boundary.

To satisfy conditions on exponential decay of the integrand along certain paths in the complex ray parameter plane, S_I is decomposed into a term representing a wave reflected from the top of the inner core boundary and a term representing all of the multiply reflected waves from the underside of the boundary:

$$S_I = S_I' + S_I'' \tag{10}$$

where S_I' and S_I'' are defined by

$$S_I' = R_i^{\curvearrowright} \left[\frac{k_{\omega p-\frac{1}{2}}^{(2)}(r_i)}{k_{\omega p-\frac{1}{2}}^{(1)}(r_i)}\right] \tag{11a}$$

$$S_I'' = T_{KI}^{\downarrow} T_{IK}^{\uparrow} \left[\frac{k_{\omega p-\frac{1}{2}}^{(2)}(r_i)}{k_{\omega p-\frac{1}{2}}^{(1)}(r_i)}\right] \left[\frac{i_{\omega p-\frac{1}{2}}^{(1)}(r_i)}{i_{\omega p-\frac{1}{2}}^{(2)}(r_i)}\right] / (1-M) \tag{11b}$$

where

$$M = R_I^{\curvearrowright} \left[\frac{i_{\omega p-\frac{1}{2}}^{(1)}(r_i)}{i_{\omega p-\frac{1}{2}}^{(2)}(r_i)}\right]. \tag{12}$$

In the expressions above $R_i^{\checkmark}$ and $R_I^{\wedge}$ are the respective reflection coefficients for a compressional wave incident on the top and bottom side of the inner core boundary; $T_{KI}^{\downarrow}$ and $T_{IK}^{\uparrow}$ the respective transmission coefficients from top and bottom side; and $k^{(2)}_{\omega p-\frac{1}{2}}$ and $i^{(2)}_{\omega p-\frac{1}{2}}$ the radial eigenfunctions in the outer and inner core evaluated at the radius r_i of the inner core. The coefficients, T_{KI}, etc. are given in the appendix as functions of ray parameter, velocities and densities in the core.

The denominator of the S_I'' term can be expanded in an infinite series of ascending powers of M, representing successively increasing numbers of reflections from the underside of the boundary. This series, originally derived by Debye (1908) for the internal reflections in a cylinder, converges rapidly for waves incident on a discontinuous velocity decrease. For a wave at or near critical incidence to a velocity increase, however, it does not converge at infinite frequency and converges poorly at finite frequency. This is because at finite frequencies and real ray parameters the magnitude of M nearly equals 1 at critical incidence. At infinite frequency $|M|$ exactly equals 1. For waves having a 2 s period at the D cusp of PKP several hundred such terms must be summed before apparent convergence is reached.

Figures 3 to 4 show the paths taken, the location of poles in the factor f, and the behavior of saddle points in the complex ray parameter plane for PKP in the distance range (110°–152°). The only constraints on the path at any distance is that it lie sufficiently near all ray theory saddle points and end in regions of exponential decay of the integrand. In the region of partial reflection (Fig. 3a) one saddle point exists at a ray parameter value less than that corresponding to critical incidence. Evaluation at this saddle point in the limit of geometrical ray theory gives the amplitude of the single wave partially reflected from the top of the inner core boundary. In the region of total reflection there exist a saddle point for the totally reflected ray at a ray parameter greater than critical and many saddle points for the multiple internal reflections that compose the interference head wave at ray parameters less than critical. These are the saddles of the term containing S_I'' after expanding its denominator. At the D cusp all of these saddles coalesce. Also shown are the ray theory saddles associated with the AB and BC branches of PKP, representing transmission through only the outer core. Beyond the caustic B near 146°, these saddles leave the real p axis (Richards, 1973) and are oriented as shown in Figure 4.

Where the contour of integration encloses poles in S_I, S_I' or S_I'' residue contributions are picked up, corresponding to rays diffracted along the inner core boundary. Two types of diffracted waves occur: those given by the residues of poles lying near the real ray parameter axis, emanating from the critical ray parameter, and those given by the residues of poles emanating upward in the first quadrant of the complex p plane from the grazing ray parameter. The former describe waves diffracted along the underside of the inner core boundary shedding energy to the exterior at an angle near the critical angle. These waves correspond to the whispering gallery modes described by Rayleigh (1910) for a liquid sphere having a rigid boundary. The latter describe waves diffracted along the top side of the inner core boundary, shedding energy upward at an angle

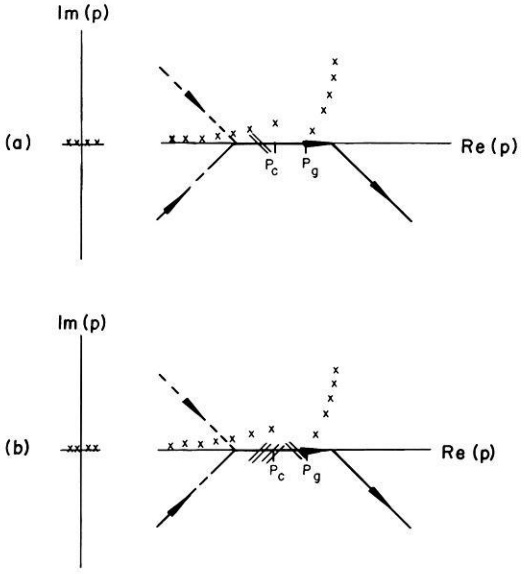

Fig. 3a and b. Paths in the complex ray parameter plane at a distance near the PKP-D cusp. The single vertical ticks along the real p axis mark the position of the critical ray parameter p_c, which grazes the underside of the inner core boundary, and the grazing ray parameter p_g, which grazes the top side of the inner core boundary. **a** The position of poles (× 's) and the position and orientation of saddles (//'s) for the region of partial reflection ($\Delta \leqq 120°$) in earth model 1066B. **b** The poles and saddles in the region of total reflection ($\Delta > 120°$). The solid line signifies that the product of reflection-transmission coefficients f contains the factor S_I, the dashed line ----- S_I' and the long dashed – short dashed line – – – S_I''

near the grazing angle. These poles were described by Franz (1957) for a liquid sphere. The whispering gallery poles are given by the zeros in the denominator of the S_I'' term. The Franz poles in the first quadrant are common to both S_I and S_I''.

The reason for combining S_I' and S_I'' to form S_I for the contour beyond the critical ray parameter follows from a criticism made by Ludwig (1970). Ludwig noted that a contour for S_I' continued beyond this point would include the contribution of additional, unphysical Franz poles in the fourth quadrant of the p plane (not shown in Figs. 3 and 4). Indeed, numerical experiments in this study confirmed Ludwig's prediction that the residue contributions of these poles lead to an exponentially growing amplitude for the S_I' term into the region of total reflection. The presence of these poles, in addition, prohibits a smooth transition from total to partial reflection in a calculation that treats the S_I' term with a separate contour.

Forming the sum $S_I' + S_I''$, however, cancels the unphysical poles in the fourth quadrant. This can be shown by considering the common denominator of S_I' and S_I'', the zeros of which give the pole positions of their sum. In terms of the radial

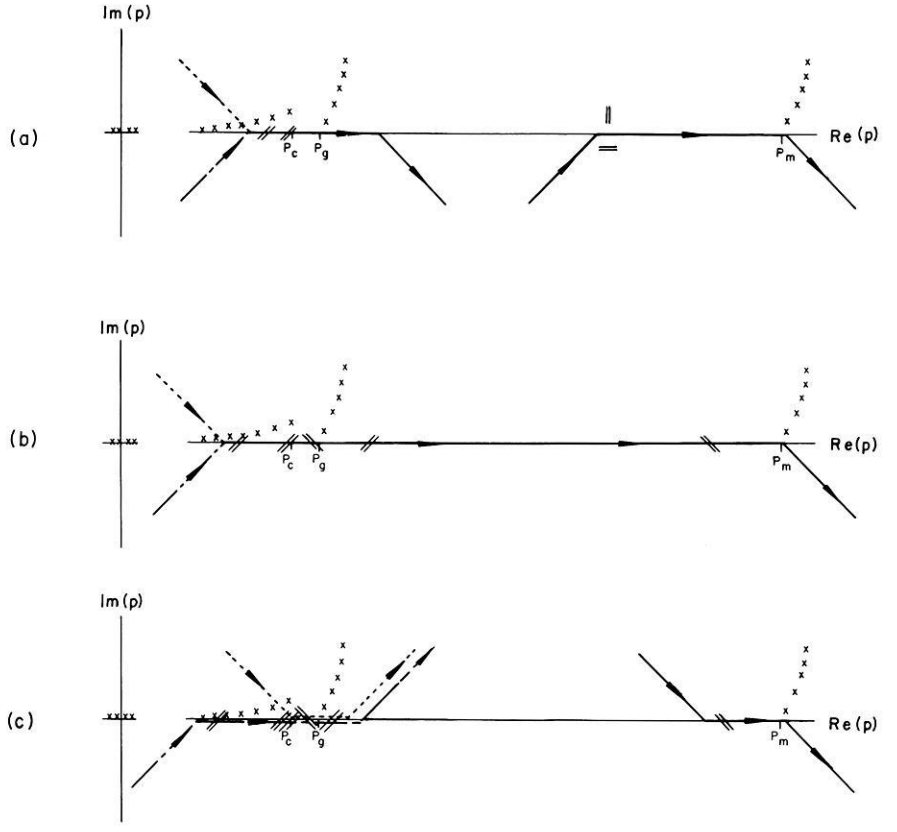

Fig. 4a–c. Paths incorporating the effect of saddles of the PKP-B caustic: **a** 128°–140°, **b** 142°–150°, 142°–150°, **c** paths for PKP at 152°. In the integrand of reflection-transmission coefficients the factor S_I' is substituted for the path --- that includes the effect of the ray theory saddles for the BC and CD branches of PKP, S_I'' for the path – · – for the DF and associated multiple internal reflection branches, and S_I for the path ——— for the AB branch. Besides the critical and grazing ray parameters and poles associated with the inner core boundary, the Franz poles and grazing ray parameter p_m in the mantle are shown for the outer core boundary

eigenfunctions, the denominator of S_I' is given by

$$D_{S_I'} = \left\{ -A\frac{i'^{(2)}}{i^{(2)}} + B\frac{k'^{(1)}}{k^{(1)}}\left[C\frac{i'^{(2)}}{i^{(2)}} + D\right]\right\} k^{(1)} \tag{13}$$

and the denominator of S_I'' by

$$D_{S_I''} = \left\{ 1 - \frac{A\dfrac{i'^{(1)}}{i^{(1)}} - B\dfrac{k'^{(1)}}{k^{(1)}}\left[C\dfrac{i'^{(1)}}{i^{(1)}} + D\right]}{-A\dfrac{i'^{(2)}}{i^{(2)}} + B\dfrac{k'^{(1)}}{k^{(1)}}\left[C\dfrac{i'^{(2)}}{i^{(2)}} + D\right]}\right\} i^{(2)} k^{(1)}, \tag{14}$$

where A, B, C and D are constants given by combinations of the velocities and densities at the inner core boundary (see appendix); and where the subscript $\omega p - \frac{1}{2}$ and the argument (r_i) is understood for the radial eigenfunctions $i^{(2)}$, $i^{(1)}$, and $k^{(1)}$. The common denominator (the denominator of S_I) is given by

$$D_{S_I} = \{ -A i'^{(2)} k^{(1)} + B k'^{(1)} [C i'^{(2)} + D i^{(2)}] - A i'^{(1)} k^{(1)} + B k'^{(1)} [C i'^{(1)} + D i^{(1)}] \} . \tag{15a}$$

Combining terms here results in

$$D_{S'_I + S''_I} = -A j' k^{(1)} + B k'^{(1)} [C j' + D j], \tag{15b}$$

where

$$j = i^{(1)} + i^{(2)}. \tag{16}$$

For a homogeneous medium $i^{(1)}$ and $i^{(2)}$ are exactly spherical Hankel functions and j a spherical Bessel function. The poles of the combined function $S_I (= S'_I + S''_I)$ now lie near the zeros of the radial eigenfunctions j and $k^{(1)}$. Those that lie near the zeros of j are the whispering gallery poles and those near the zeros of $k^{(1)}$ the Franz poles in the first quadrant. Additional Franz poles in the fourth quadrant near the zeros of $i^{(2)}$, which are present in the S'_I function, are no longer present in the combined S_I function.

For the contour taken in the distance range 110°–126° (Fig. 3) only the ray interactions with the inner core boundary are important. From 128°–150° the additional contour in Figure 4a and the extended contour in Figure 4b include the contribution of a low frequency phase given by the imaginary saddle points in the shadow of the PKP-B caustic. Buchbinder (1974) described this phase as "diffraction from the B caustic" and identified it on seismograms in the distance range 128°–142°.

Because both the arrival times and saddles of the inner core interactions are well separated from those of the B caustic diffraction in the distance range 128°–140°, it is convenient to calculate these phases by two separate paths (Fig. 4a). The result of each integration can have a different arrival time ramp removed before the inverse Fourier transform is taken for synthesis in the time domain. A theoretical seismogram can then be formed by summing the two time signals, lagging the earlier one by the difference in the arrival time ramps.

From 142°–150° some of the ray theory saddles are well separated, but the arrival times of all phases are sufficiently close that where S'_I and S''_I are combined, a single contour (Fig. 4b) may be taken for calculation of all the PKP branches. At 152° separate contours are taken (Fig. 4c) for (i) the phases reflected and diffracted along the top of the inner core boundary that produce point C on the PKP $T-\Delta$ curve, (ii) the combined transmitted and internally reflected phases in the inner core that produce the DF and associated infinite series of branches, (iii) and the phase simply transmitted through the outer core that gives the AB branch.

Alternative to the multiple contours taken in certain distance ranges (Fig. 4b and 4c), a single countour where S'_I and S''_I are combined, could always have

been taken. For the distance ranges in which certain phases are well separated in arrival time, however, calculations at many more frequencies would have been required to sample correctly the modulation of the phase and amplitude spectrum of the Fourier transformed signal.

For integration at ray parameters corresponding to waves bottoming above the inner core boundary, the factor S_I was retained in the integrand of reflection-transmission coefficients. This was possible because the Langer approximation allows S_I to go smoothly to 1 in this range of ray parameters.

Incorporation of Attenuation

Since the solution formulae are all analytic in velocity, the solution for an attenuating earth is given by analytic continuation to a complex velocity profile defined in terms of a Q and real velocity model (Cormier and Richards, 1976). For the Q model in this study, a constant Q of 5000 was taken for the mantle, 20,000 for the outer core, and 1000 for the inner core. As Müller (1973) predicted in his study of the inner core, the Q model chosen did not observably effect the amplitudes of long period synthetic seismograms. This was true of even the more highly attenuating Q model of Doornbos (1974) for the top of the inner core. Only at periods shorter than 2 s was the effect of such a low Q zone manifest. Because in principle attenuation can effect the amplitude of waves interacting with boundaries (Kennett, 1975) and because its incorporation involved no additional computational difficulty, the calculations nevertheless included the simple Q model above.

Earth Models Considered

Theoretical seismograms were calculated for PKP in earth models C2, 1066B, and PEM. Figure 5 compares these models in the earth's core. All of the models have virtually the same S velocity distribution in the inner core, corresponding to an average of 3.5 km/s but with a positive gradient with increasing depth. The density increase (0.2 gm/cm^3) at the inner core boundary is smallest for Anderson and Hart's (1976) model C2, which followed from their hypothesis that the inner core boundary simply marks the solid-liquid phase boundary in a materially homogeneous core. The P velocity distribution in C2, having a jump of 0.56 km/s at the inner core boundary and pronounced gradient at the top of the inner core, is essentially that suggested by Müller's (1973) study. Model 1066B (Gilbert and Dziewonski, 1975) has a P velocity jump of 0.67 km/s and density jump of 0.56 gm/cm^3 at the inner core boundary. The PEM model resulted from the study of Dziewonski et al. (1975), who noted that models such as 1066B, which specify model parameters on discrete radii, generally show minor perturbations in gradients that are inconsistent with a hypothesis of homogeneity in the lower mantle and core. The three PEMs (-0, $-C$, and $-A$), differing only in taking an oceanic, continental, or average structure for the upper mantle, give velocities and densities as simple analytic functions of

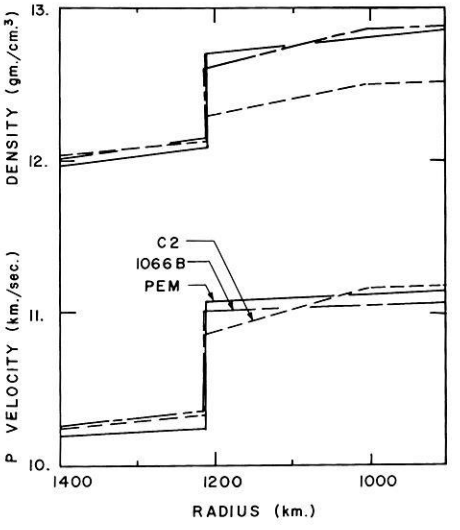

Fig. 5. Velocity and density models of the inner core by 1066B, PEM, and C2. An anomalous density gradient at the top of the inner core is given by 1066B, and both an anomalous *P* velocity and density gradient by C2

radius over large regions of depth. These functions are low order polynomials. The velocity and density distribution for the cores is consistent with the hypothesis of homogeneity. The PEMs have a velocity jump of 0.83 km/s and density jump of 0.57 gm/cm^3 at the inner core boundary.

Results

Synthetics

Theoretical seismograms calculated in PEM-A are shown in Figures 6–9. The impulse response for PKP, shown in Figure 6, was convolved with the source pulses given by Müller (1973) for three shallow focus earthquakes (sources 1 to 3). Figure 7 compares the resultant synthetics with the WWSSN records of source 3. An alternate procedure was found to be adequate for two deep focus earthquakes (sources 4 and 5). The synthetics in these cases were calculated by convolving the impulse response with a WWSSN response and a boxcar function to model the earthquake source time function. The two deep focus earthquakes (Figs. 8 and 9) provide more detail on structural modulation of the waveform because they do not possess the strong crustal reverberations of the shallow focus earthquakes that effectively act to lengthen the source pulse. The complexity of many interfering phases between 142° and 152° is not reflected in complexity of waveform when the time duration of the source pulse is long compared to the time separation of the interfering phases.

The diffracted phase from the B caustic produces the low frequency precursor in the distance range 128°–140°, in agreement with the identification of Buchbinder (1974). The slowness of this phase for the theoretical seismograms is 3.5 s/deg. This value was inferred from both the arrival time ramps removed

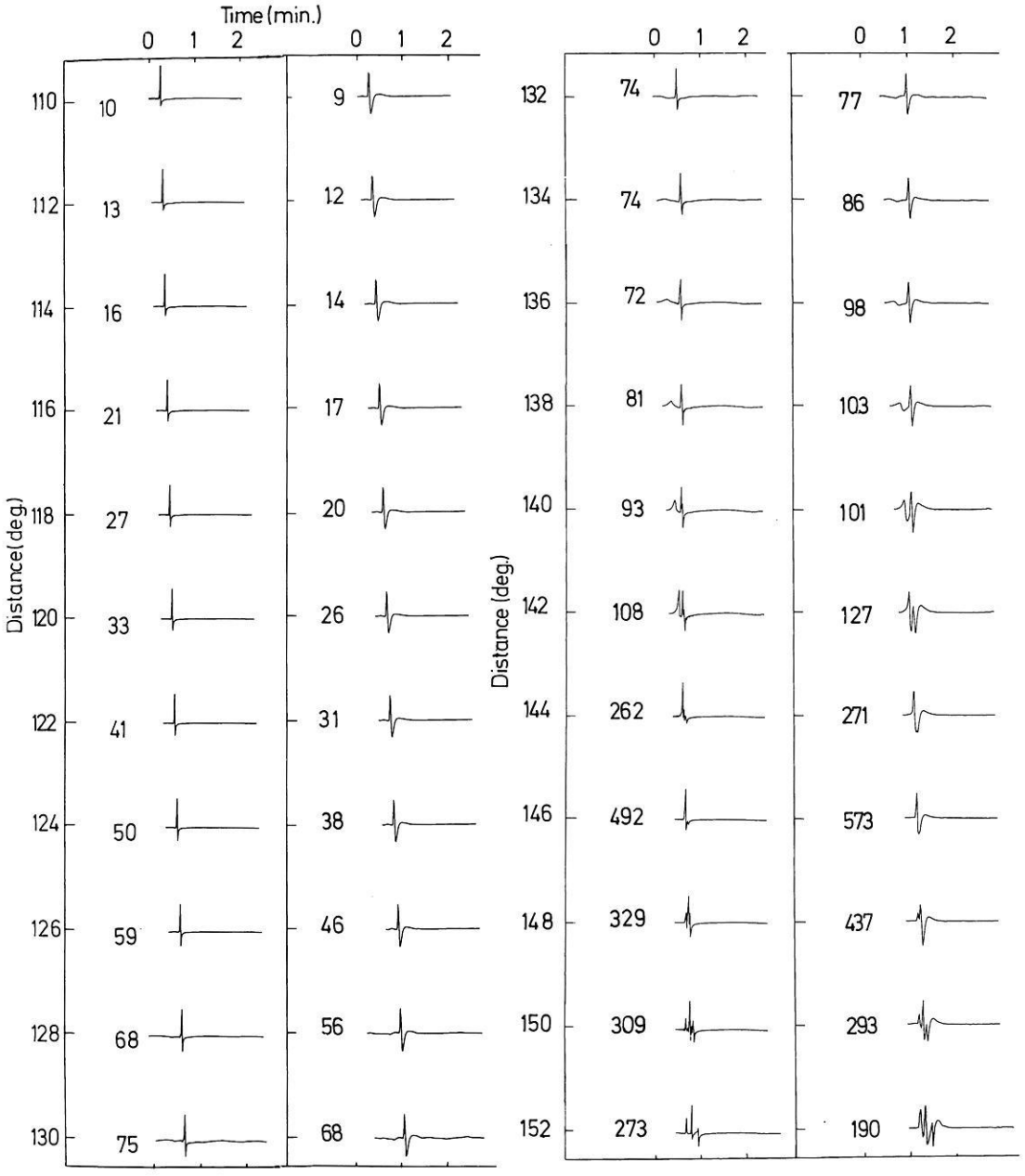

Fig. 6. Left: impulse response for PKP in the PEM earth model; right: impulse response convolved with the response of a 15–100 WWSSN vertical seismograph. Numbers at the left of responses indicate relative amplitude in a sequence of increasing distances. Note that the waveform does not change across the critical point near 120 degrees. The position of the critical point merely effects amplitudes

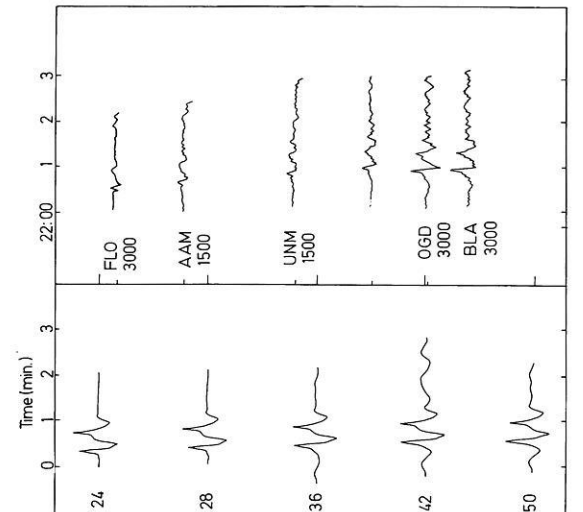

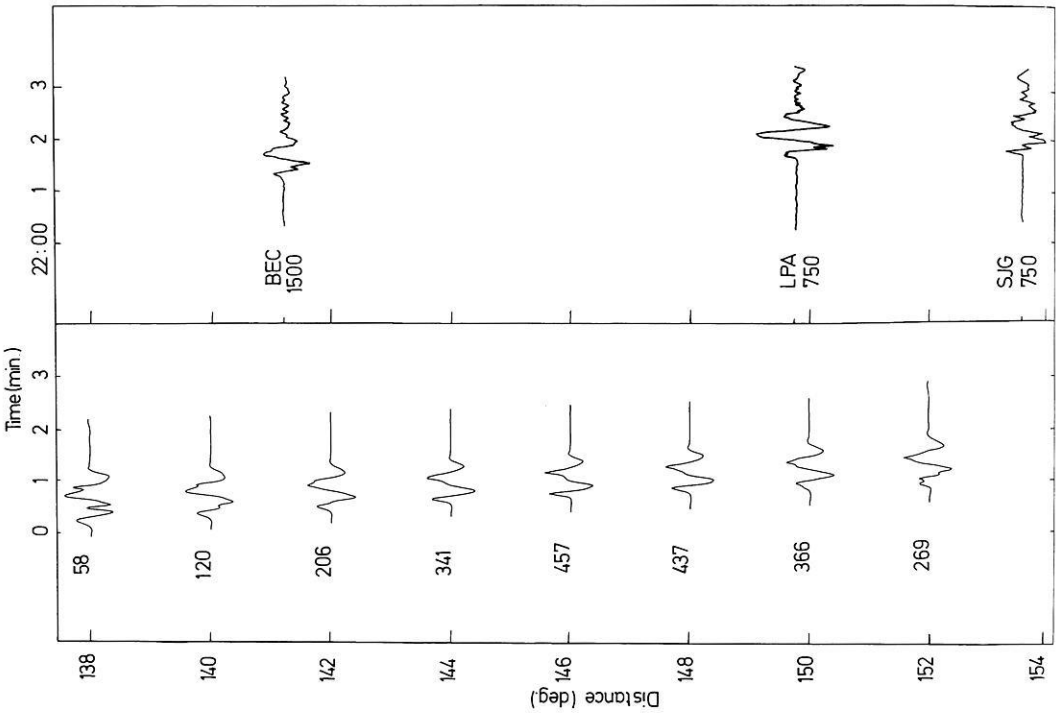

Fig. 7. Comparison of theoretical seismograms for PKP in PEM with earthquake seismograms for Müller's (1973) source no 3 (Feb. 3, 1969; 21:41:41.9 G.M.T.; 4.9° N, 127.3° E; 30 km). Theoretical seismograms in the left column, numbers indicating relative amplitude in distance range. Actual seismograms in the right column, three letter station code and peak magnification noted

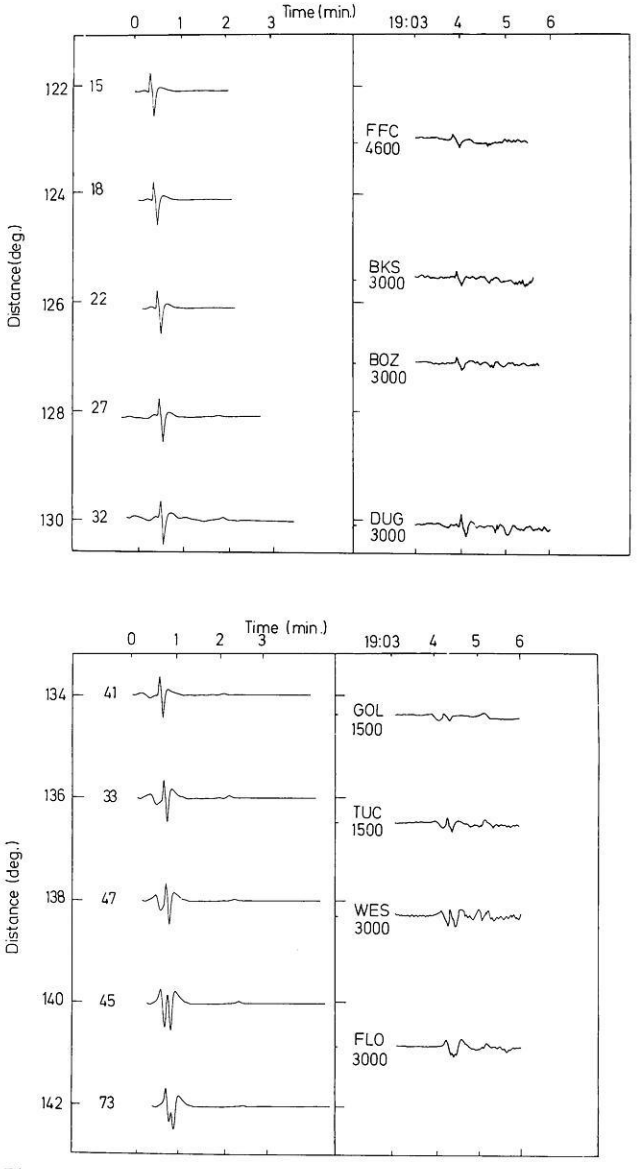

Fig. 8. Comparison for source no. 4 (May 21, 1967; 18:45:11.7 G.M.T.; 1.0° S, 101.5° E; 173 km)

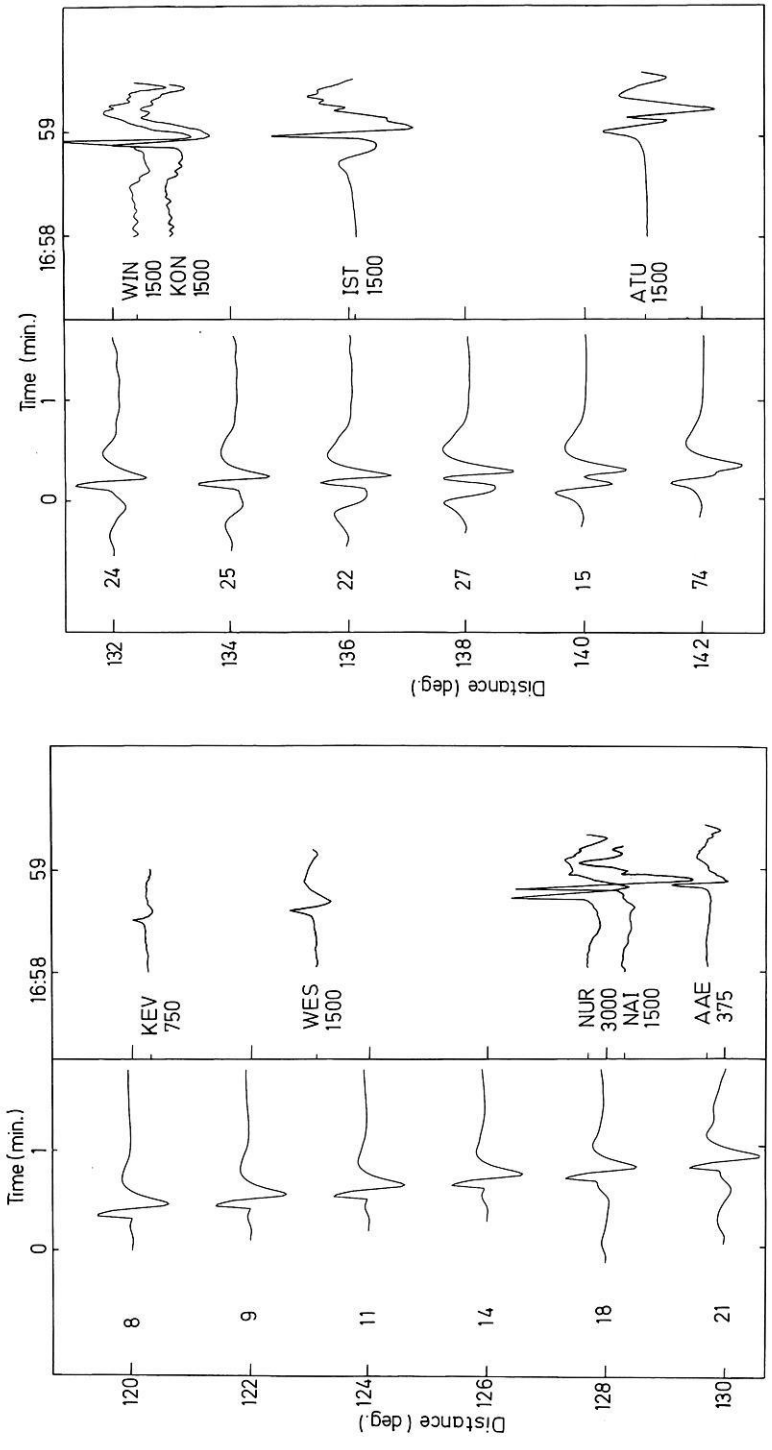

Fig. 9. Comparison for source no. 5 (July 9, 1964; 16:39:49.3 G.M.T.; 15.5° S, 167.6° E; 121 km)

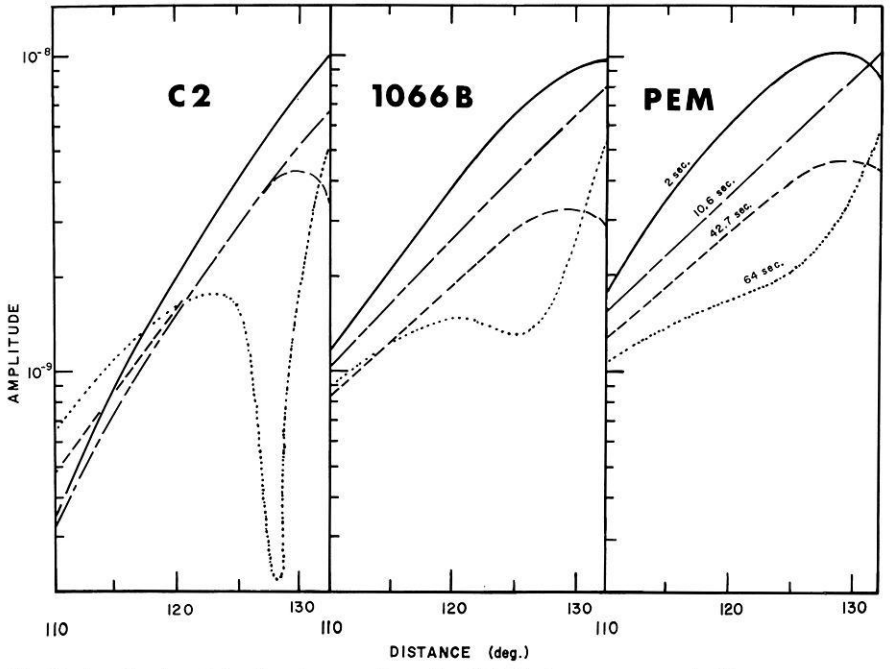

Fig. 10. Amplitudes of the Fourier-transformed radial displacement near the D cusp

before Fourier inversion and by direct calculation of phase slowness in the frequency domain. The slowness has little dispersion up to 20 s period.

Amplitudes in the Frequency Domain near the D-Cusp

Figure 10 summarizes amplitude calculations in the frequency domain for earth models C2, 1066B, and PEM-A. In each model the amplitude near critical incidence is less for lower frequencies. If in fact the Debye ray series converges at infinite frequency, the assumption of simple geometric ray theory and plane wave reflection coefficients would predict a curve near the shortest period curves (2 s) in Figure 10. Thus, the magnitude of a velocity increase inferred from amplitude measurements at long periods near a cusp at critical incidence will be erroneously small by neglecting the frequency dependence due to the effects of boundary curvature and radial inhomogeneity near the boundary. The growth of low frequency amplitudes for PKP beginning at 130° reflects the growing contribution of the phase diffracted from the B caustic. Low frequency amplitudes are less in the PEM-A model than in the discrete earth models C2 and 1066B. In the discrete earth models the low frequency amplitudes grow large again at shorter distances corresponding to partial reflection. These differing results at low frequencies in the discrete earth models may be an effect of the

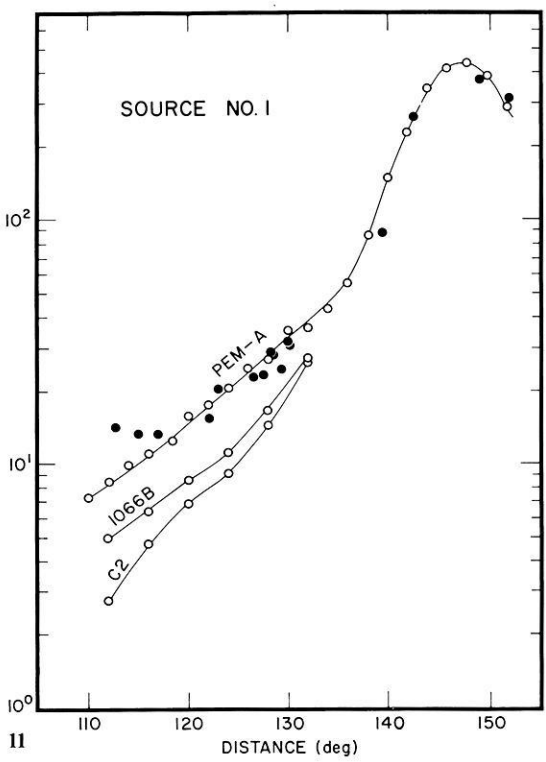

11

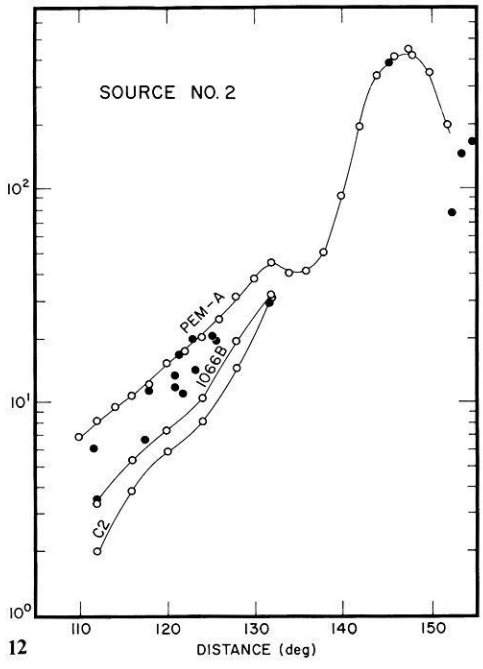

12

Fig. 11. Amplitude curves for theoretical seismograms of PKP in the earth models PEM (110°–152°), 1066*B* and *C*2 (112°–132°) (○'s) with Müller's source no. 1 compared with amplitudes (●'s) measured from WWSSN seismograms of earthquake source no. 1 (Jan. 10, 1970; 6.8° N, 126.7° E; 73 km). Amplitude is in arbitrary units measured on a seismogram, normalited to the peak amplitude near 145°

Fig. 12. Amplitude comparison for source no. 2 (April 7, 1970; 15.8° N, 121.7° E; 30 km)

longer integration paths required for the low frequency calculations. A portion of these longer paths correspond to rays that bottom near the center of the earth at which the Mohovoričić velocity interpolation law used in calculating ξ and J for the discrete earth models fails. The failure can be seen in Equation (8). For a positive velocity gradient with increasing depth ($b_i < 0$), Equation (8) has $\alpha \to \infty$ as $r \to 0$.

Amplitudes in the Time Domain

Peak to peak amplitudes of the theoretical seismograms were compared to the amplitudes of earthquake seismograms by Müller's (1973) amplitude method, in which all amplitudes are normalized to the peak amplitude near the B caustic between 146°–148°. Figures 11 to 15 illustrate the results of this comparison for Müller's earthquake sources. The amplitudes of seismograms were reread, and

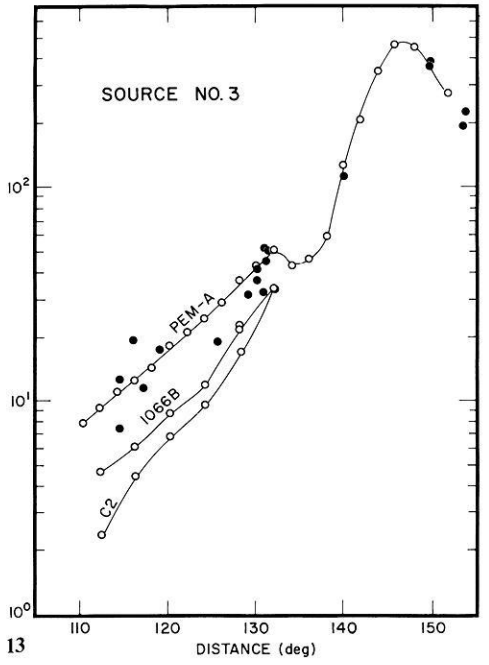

13

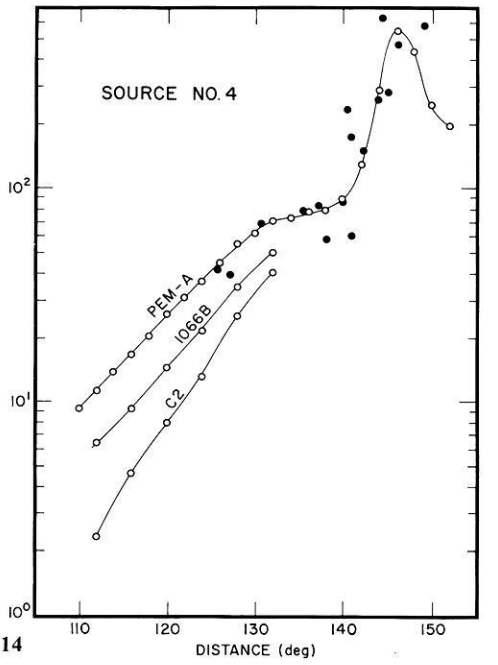

14

Fig. 13. Amplitude comparison for source no. 3 (Feb. 3, 1969; 4.9° N, 127.3° E; 30 km)

Fig. 14. Amplitude comparison for source no. 4 (May 21, 1967; 1.0° S, 101.5° E; 173 km)

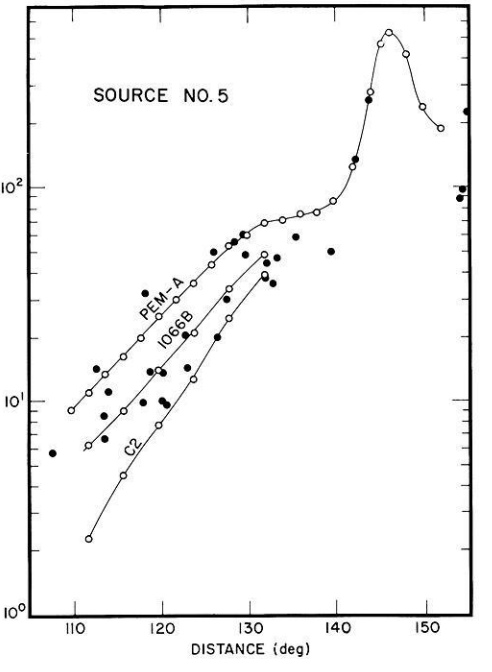

Fig. 15. Amplitude comparison for source no. 5 (July 9, 1964; 15.5° S, 167.6° E; 121 km)

adjusted by corrections indicated by calibration pulse amplitudes. The data show more scatter than the same data shown by Müller (1973). More data at 110°–120° with lower signal to noise ratio, however, are plotted. Amplitude data of sources 1, 3 and 4 lie close to those predicted by PEM-A. Those of source 2 lie between the curves of PEM and 1066B and those of source 5 scatter above C2. Because the main intent of this study was to develop and extend a technique for calculations near critical incidence, no attempt was made to explore the bounds on the infinite family of core models that satisfy the data. It was ascertained, however, that the lower amplitudes of the C2 model near the D cusp arose from the smaller P velocity jump and not from the smaller density jump at the inner core boundary. Consequently, from the fit of the PEM predicted to the observed amplitudes, it can be concluded (i) that the long period PKP amplitudes do not require an anomalous P velocity gradient at the top of the inner core, (ii) that a P velocity jump as high as 0.83 km/s is consistent with the data, and (iii) that Dziewonski et al.'s (1975) hypothesis of homogeneity and adiabaticity in the earth's core is not rejected by this data set.

Discussion

Comparison with Previous Studies in Full Wave Theory

This study differs from previous studies in the decision not to make the Debye ray expansion at and near critical incidence. Nussenzveig (1969) chose to make the Debye expansion for the case of ray interactions with both a discontinuous velocity decrease and increase. He treated each term in the Debye expansion separately, choosing for each an integration path in the complex order plane. Nussenzveig's function S for a discontinuous velocity increase is the liquid-liquid analog of our function S_I for a compressional wave incident on the liquid-solid boundary of the inner core-outer core boundary of the earth. His decision to expand the S function in the Debye series was motivated by the slow convergence of the residue series associated with the whispering gallery poles of the S function. Ludwig (1970) and Überall (1975), however, noted that the Debye series itself converges slowly at and near critical incidence to a velocity increase.

This study uses contours in the complex ray parameter plane and a decomposition of the S function similar to those of Ludwig (1970) in the complex order plane. Ludwig (1970) and Überall (1975) chose to evaluate the integral representation of displacement in terms of separate saddle point and residue contributions. Ludwig noted the difficulty of separating these two types of contributions and suggested that the integration contour be adjusted so that the last residue included is of the same order as the last saddle. The numerical integration along the contour of this study, however, properly includes the effects of poles and saddles without readjusting the contour at each distance and frequency. The contour taken in the complex ray parameter plane is appropriate over a wide range of distances and frequencies. The effect of higher order whispering gallery poles increases with increasing frequency as more poles pack close to the contour along the real axis. At a given frequency the magnitude of

the residue contribution of each pole is governed by the distance Δ_0 in the phase factor J, higher order poles becoming more important farther into the zone of total reflection.

Because the S velocity in the mantle is less than that of compressional waves in the outer core, Choy's (1977) SKS study is also an example of waves incident on a discontinuous velocity increase. The distance range (100°–120°) in which Choy chose to synthesize the SKS and SmKS phases was far enough away from the distance point of critical incidence of SV on the core-mantle boundary (60°) that only a small number of terms of the Debye ray series needed to be summed for the total amplitude. Choy reported, however, that the series for SmKS began to show poor convergence for $m>6$. Choy's results suggest the convenience of making a progressive expansion of the Debye series farther from critical incidence, treating separately in a ray parameter integrand those terms well separated in arrival time, but lumping together as an interference head wave higher order terms that arrive nearly simultaneously and converge slowly. Thus, far from the PKP-D cusp in the lit zone, the function S_I can be expanded as

$$S_I = R_i^{\swarrow} \frac{k^{(2)}_{\omega p-\frac{1}{2}}(r_i)}{k^{(1)}_{\omega p-\frac{1}{2}}(r_i)} + T_{KI}^{\downarrow} T_{IK}^{\uparrow} \frac{k^{(2)}_{\omega p-\frac{1}{2}}(r_i)}{k^{(1)}_{\omega p-\frac{1}{2}}(r_i)} \frac{i^{(1)}_{\omega p-\frac{1}{2}}(r_i)}{i^{(2)}_{\omega p-\frac{1}{2}}(r_i)} \sum_{m=0}^{N} \left[R_I^{\curvearrowleft} \frac{i^{(1)}_{\omega p-\frac{1}{2}}(r_i)}{i^{(2)}_{\omega p-\frac{1}{2}}(r_i)} \right]^m$$
$$+ T_{KI}^{\downarrow} T_{IK}^{\uparrow} \frac{k^{(2)}_{\omega p-\frac{1}{2}}(r_i)}{k^{(1)}_{\omega p-\frac{1}{2}}(r_i)} \frac{i^{(1)}_{\omega p-\frac{1}{2}}(r_i)}{i^{(2)}_{\omega p-\frac{1}{2}}(r_i)} \sum_{m=N+1}^{\infty} \left[R_I^{\curvearrowleft} \frac{i^{(1)}_{\omega p-\frac{1}{2}}(r_i)}{i^{(2)}_{\omega p-\frac{1}{2}}(r_i)} \right]^m . \tag{17}$$

The first term on the right of Equation (17) and the terms in the seires $\sum_{m=0}^{N}$ can be treated as separate problems of integration in the complex ray parameter plane. The remainder summation $\sum_{m=N+1}^{\infty}$ can be dropped if it is demonstrably small but can without additional difficulty be included in a single integration problem by calculating it in terms of the finite sum and the total sum S_I'', i.e.,

$$T_{KI}^{\downarrow} T_{IK}^{\uparrow} \frac{k^{(2)}_{\omega p-\frac{1}{2}}(r_i)}{k^{(1)}_{\omega p-\frac{1}{2}}(r_i)} \frac{i^{(1)}_{\omega p-\frac{1}{2}}(r_i)}{i^{(2)}_{\omega p-\frac{1}{2}}(r_i)} \sum_{m=N+1}^{\infty} \left[R_I^{\curvearrowleft} \frac{i^{(1)}_{\omega p-\frac{1}{2}}(r_i)}{i^{(2)}_{\omega p-\frac{1}{2}}(r_i)} \right]^m$$
$$= S_I'' - T_{KI}^{\downarrow} T_{IK}^{\uparrow} \frac{k^{(2)}_{\omega p-\frac{1}{2}}(r_i)}{k^{(1)}_{\omega p-\frac{1}{2}}(r_i)} \frac{i^{(1)}_{\omega p-\frac{1}{2}}(r_i)}{i^{(2)}_{\omega p-\frac{1}{2}}(r_i)} \sum_{m=0}^{N} \left[R_I^{\curvearrowleft} \frac{i^{(1)}_{\omega p-\frac{1}{2}}(r_i)}{i^{(2)}_{\omega p-\frac{1}{2}}(r_i)} \right]^m . \tag{18}$$

Extension to Other Problems

The decomposition of the S function and the path Γ discussed in this paper can be used as a guideline for application to other problems involving waves at or near critical incidence. With this method, for example, the amplitude of P_n and other crustal refractions would remain valid at critical incidence, offering an important advantage over the method described by Hill (1971).

The results for PKP demonstrated that it is not difficult to apply the Langer approximation simultaneously to the reflection-transmission coefficients associated with two or more boundaries. A transition zone may be modeled most

simply by a sequence of first order discontinuities separating radially inhomogeneous layers. The number of discontinuities required to describe the transition zone will be a function of frequency such that in each inhomogeneous layer wave propagation can be adequately described by simple Helmholtz equations for SH and decoupled P-SV potentials (Richards, 1974). The results for PKP indicate that the product of the Langer approximated S functions of such a transition zone will be a smooth function in the complex ray parameter plane. If the transition zone were alternatively modeled as a single inhomogeneous layer sandwiched between two thick layers of less intense velocity gradient, then a higher order Langer approximation would be required for the radial eigenfunctions of the complete second order wave equations satisfied by the SH and coupled P-SV potentials.

Conclusions

The full wave theory described by Richards (1973) for wave interactions with velocity decrease has been extended to a velocity increase. The method is modified only by the choice of the integrand of reflection-transmission coefficients and the path in the complex ray parameter plane. By not choosing, in general, to make the Debye ray expansion the method successfully accounts for all of the waves in the high velocity medium that are repeatedly refracted back to, and reflected from, the low velocity medium. Not making the Debye expansion essentially amounts to calculating a reflection-transmission coefficient S that allows reflected-transmitted waves to exist in both the same and opposite radial direction as the incident wave. The method is valid at critical incidence to a velocity increase and predicts a smooth, uncomplicated transition in amplitude and waveform from the zone of partial to total reflection.

Results of calculating synthetic seismograms for PKP indicate that the amplitude maximum associated with critical incidence at the D cusp is less at lower frequencies and displaced farther into the zone of total reflection. Consequently, erroneously small velocity jumps or anomalous velocity gradients at the inner core boundary will be inferred from the assumption of the validity of simple geometric ray theory and plane wave reflection-transmission coefficients near and at critical incidence. Theoretical seismograms calculated in Dziewonski et al.'s (1975) PEM model for the earth's core agree in amplitude and waveform with observed seismograms, suggesting that the hypothesis of homogeneity and adiabaticity of the earth's core cannot be rejected at the wavelengths of long period body waves.

Appendix

Reflection-Transmission Coefficients

In terms of the velocities and densities at the radius r_i of the inner core, the reflection-transmission coefficients associated with interactions with the inner

core boundary are given by

$$
\begin{aligned}
T_{KI}^{\downarrow} &= [\rho_2(\alpha_1/\alpha_2)\, v_1(C_{i2}^{(1)} + C_{i2}^{(2)})]/D_{S_I'} \\
T_{IK}^{\uparrow} &= [\rho_1\, v_1(C_{i1}^{(1)} + C_{i2}^{(2)})]/D_{S_I'} \\
R_i^{\curvearrowright} &= [-\rho_2\, C_{i1}^{(2)} + (\rho_1/\alpha_2)\, C_{i2}^{(2)}(\alpha_1\, v_1^2 + 4\beta_4^3\, p^2/r_i^2\, C_{i1}^{(2)}\, C_{j1}^{(2)})]/D_{S_I'} \\
R_I^{\curvearrowright} &= [\rho_2\, C_{i1}^{(1)} + (\rho_1/\alpha_2)\, C_{i2}^{(1)}(-\alpha_1\, v_1^2 + 4\beta_1^3\, p^2/r_i^2\, C_{i1}^{(1)}\, C_{j1}^{(2)})]/D_{S_I'} \\
S_I &= [-\rho_2\, C_{i1}^{(1)+(2)} + (\rho_1/\alpha_2)\, C_{i2}^{(2)}(\alpha_1\, v_1^2 + 4\beta_1^2\, p^2/r_i^2\, C_{i1}^{(1)+(2)}\, C_{j1}^{(2)})]/D_{S_I}
\end{aligned}
\tag{A1}
$$

where

$$
\begin{aligned}
v_1 &= (1 - 2\beta_1^2\, p^2/r_i^2), \\
D_{S_I'} &= [\rho_2\, C_{i1}^{(2)} + (\rho_1/\alpha_2)\, C_{i2}^{(1)}(\alpha_1\, v_1^2 + 4\beta_1^3\, p^2/r_i^2\, C_{i1}^{(2)}\, C_{j1}^{(2)})],
\end{aligned}
$$

and

$$
D_{S_I} = [\rho_2\, C_{i1}^{(1)+(2)} + (\rho_1/\alpha_2)\, C_{i2}^{(1)}(\alpha_1\, v_1^2 + 4\beta_1^3\, p^2/r_i^2\, C_{i1}^{(1)+(2)}\, C_{j1}^{(2)})].
$$

Note that form of S_I is the same as that of $R_i^{\curvearrowright}$ but with

$$
C_{i1}^{(2)} \rightarrow C_{i1}^{(1)+(2)}.
$$

The coefficients associated with interactions with the outer core-mantle boundary r_m are given by

$$
\begin{aligned}
T_{PK}^{\downarrow} &= \rho_2\, v_2(C_{i2}^{(1)} + C_{i2}^{(2)})/D_{S_K'} \\
T_{KP}^{\uparrow} &= \rho_1(\alpha_2/\alpha_1)\, v_2(C_{i1}^{(1)} + C_{i1}^{(2)})/D_{S_K'}
\end{aligned}
\tag{A2}
$$

where

$$
D_{S_K'} = [\rho_1\, C_{i2}^{(1)} + (\rho_2/\alpha_1)\, C_{i1}^2(\alpha_2\, v_2^2 + 4\beta_2^3/p^2\, r_m^2\, C_{i2}^{(1)}\, C_{j2}^{(1)})].
$$

In the equations above ρ_n, α_n, β_n are the density, P velocity and S velocity in medium n, where $n=2$ in the upper medium and 1 in the lower medium, and p is the ray parameter. In Equation (A2) the upper and lower media are the lower mantle and outer core respectively and in Equation (A1) the outer and inner cores respectively.

The generalized cosines $C_{in}^{(1)}$ and $C_{in}^{(1)+(2)}$ are for upgoing (1) downgoing (2) or both up and downgoing waves (1)+(2). The subscript i for a $C_{in}^{(1)}$ refers to a P wave and the subscript j in a $C_{jn}^{(1)}$ to a S wave. In terms of the radial eigenfunctions $g_{\omega p-\frac{1}{2}}^{(1)}$ they are defined by

$$
\begin{aligned}
C_{in}^{(1)} &= [v_n/(+i\omega)]\,[g_{\omega p-\frac{1}{2}}^{\prime(1)}(r)/g_{\omega p-\frac{1}{2}}^{(1)}(r)] \\
C_{in}^{(2)} &= [v_n/(-i\omega)]\,[g_{\omega p-\frac{1}{2}}^{\prime(2)}(r)/g_{\omega p-\frac{1}{2}}^{(2)}(r)] \\
C_{in}^{(1)+(2)} &= [v_n/(-i\omega)]\left[\frac{g_{\omega p-\frac{1}{2}}^{\prime(1)}(r) + g_{\omega p-\frac{1}{2}}^{\prime(2)}(r)}{g_{\omega p-\frac{1}{2}}^{(1)}(r) + g_{\omega p-\frac{1}{2}}^{(2)}(r)}\right]
\end{aligned}
\tag{A3}
$$

where v_n is the velocity at a radius r in medium n of a wave type i. The prime (') indicates the radial derivative. In Equations ($A1$) and ($A3$) the generalized cosines are evaluated at the radius of a boundary (r_i or r_m).

The Langer Approximation

Langer's (1949) uniformly asymptotic approximation to the radial eigenfunctions are given by Richards (1976) as

$$g^{(j)}(\omega, r, p) = \frac{A_j \xi^{\frac{1}{2}} H_{\frac{1}{3}}^{(j)}(\omega \xi)}{r[1/v^2(r) - p^2/r^2]^{\frac{1}{4}}} \tag{A4}$$

where $H_{\frac{1}{3}}^{(j)}$ is a Hankel function of the j-th kind and $\frac{1}{3}$ order; A_j is independent of r and chosen to make $g^{(j)}$ a spherical Hankel function of order $\omega p - \frac{1}{2}$ and argument $\omega r/v(r)$ in the limit of a homogeneous medium. The argument ξ in terms of velocity profile $v(r)$ is given by

$$\xi = \int_{r_p}^{r} [1/v^2(r) - p^2/r^2]^{\frac{1}{2}} dr, \tag{A5}$$

where r_p is the turning point radius. The resulting corrections in the cosines within a plane wave reflection-transmission coefficient are of the form

$$\cos\theta \to \cos\theta \, e^{-i\pi/6} H_{\frac{2}{3}}^{(1)}(\omega \xi)/H_{\frac{1}{3}}^{(1)}(\omega \xi) \tag{A6}$$

for the generalized cosine $C_{in}^{(1)}$ of an upgoing plane wave

$$\cos\theta \to \cos\theta \, e^{+i\pi/6} H_{\frac{2}{3}}^{(2)}(\omega \xi)/H_{\frac{1}{3}}^{(2)}(\omega \xi)$$

for the generalized cosine $C_{in}^{(2)}$ of a downgoing plane wave.

The cosine $C_{in}^{(1)+(2)}$ is given in the Langer approximation by

$$\cos\theta \to \cos\theta \frac{e^{-i\pi/3} H_{\frac{2}{3}}^{(2)}(\omega \xi) - e^{i\pi/3} H_{\frac{2}{3}}^{(1)}(\omega \xi)}{e^{+i\pi/6} H_{\frac{1}{3}}^{(1)}(\omega \xi) + e^{-i\pi/6} H_{\frac{1}{3}}^{(2)}(\omega \xi)}.$$

When a boundary condition is satisfied in terms of radial eigenfunctions, the factor f in Equation (7) also includes the ratios of radial eigenfunctions $[k^{(2)}/k^{(1)}]$ etc. For regions of the complex ray parameter plane in which ray theory is valid, these ratios can be incorporated into the phase factor $J(r, p)$ in Equation (7). For the Langer approximated coefficients used in this study J was calculated by assuming the wave bottoms in the velocity profile of the mantle. The ratios of the radial eigenfunctions are given accurately everywhere in the complex ray parameter plane by the Langer approximation and act to correct the phase factor J.

Frequency Behavior in Coefficients

Figures A1 to A3 illustrate the frequency dependence of the reflection-transmission coefficients associated with ray interactions with the inner core. The range shown contains the ray parameters corresponding to grazing in-

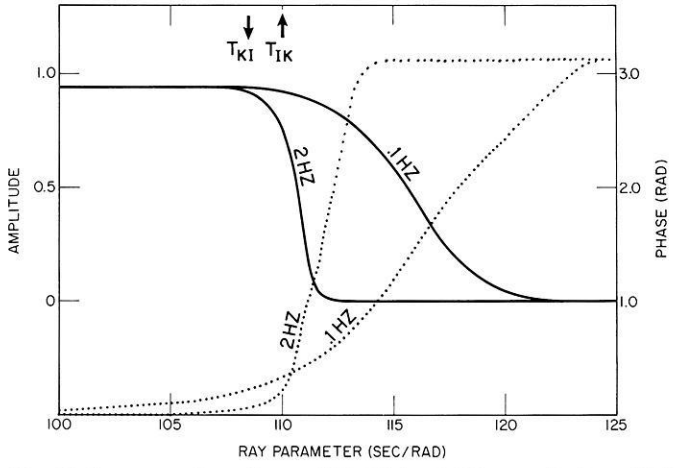

Fig. A1. Frequency dependence of $T_{KI}^{\downarrow}\, T_{IK}^{\uparrow}$ in 1066 B. Amplitude (solid lines) and phase (dotted lines) are shown at two frequencies

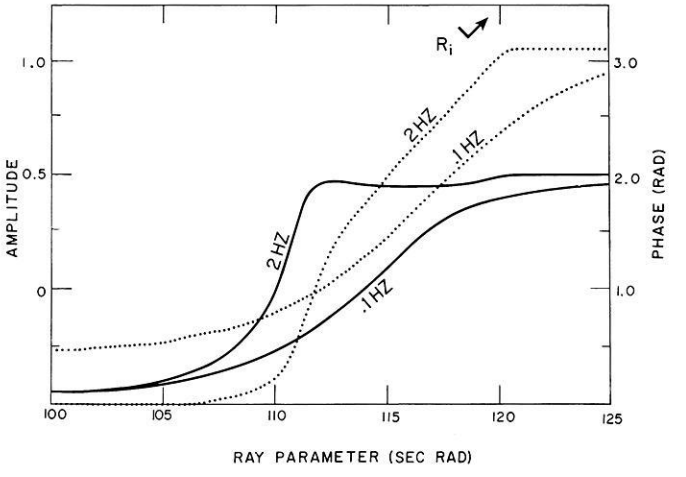

Fig. A2. Frequency dependence of $R_i^{\searrow}$ in Earth model 1066 B

cidence from the underside of the boundary ($p = 110$ rad/s) and the topside ($p = 118$ rad/s) in earth model 1066 B. The amplitude of the combined transmission coefficient through the inner core (Fig. A 1) does not vanish at ray parameters corresponding to rays that bottom above or that are totally reflected from the boundary. This behavior, however, is not strictly the tunnelling phenomena described by Richards (1973) for waves interacting with a velocity decrease. It indicates that an interaction with the underside of the boundary is possible for rays bottoming at or above the boundary. The behavior of the reflection coefficient from above the boundary, $R_i^{\nearrow}$ in Figure A 2, is similar to that of the reflection coefficient from the underside of the boundary $R_I^{\curvearrowright}$ in Figure A 3. The

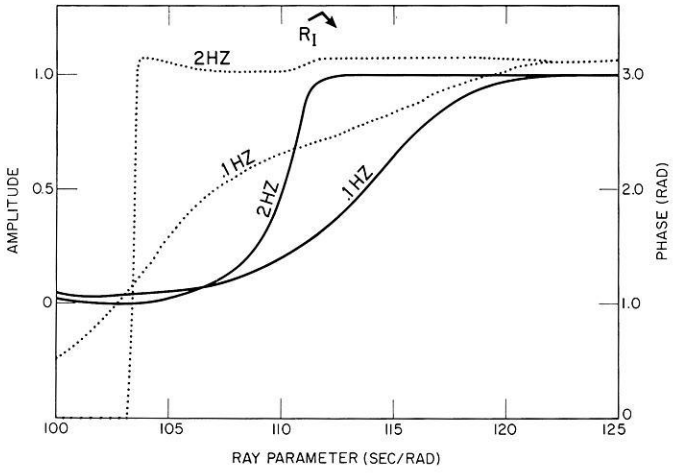

Fig. A3. Frequency dependence of $R_1\hat{}$ in 1066 B

transition from partial to total reflection in both cases is broader and occurs over a greater ray parameter range at lower frequencies. Amplitude corrections to the plane wave reflection coefficients are greatest near critical incidence ($p = 110$ rad/s), but corrections to phase are important over a broad range of ray parameters between critical and grazing. A zero in the reflection coefficient R_1 is suppressed at finite frequency for real ray parameters.

Acknowledgements. We thank Drs. L. Alsop and K. Hunkins for their critical review of the first draft. George Choy provided a program for removal of the arrival time ramp and Fourier inversion necessary for the construction of the theoretical seismograms. Linda Murphy typed the manuscript. Some of the computations in the frequency domain were carried out on an IBM 360-95 at NASA's Goddard Institute of Space Sciences, which also donated the computing time. Research was supported by the Division of Earth Sciences, National Science Foundation, NSF Grants GA 34109 and EAR-76-13136. This study was submitted in partial fulfillment of requirements for the first author's Ph.D. degree at Columbia University.

References

Anderson, D.L., Hart, R.S.: An earth model based on free oscillations and body waves. J. Geophys. Res. **81**, 1461–1475, 1976

Buchbinder, G.G.R.: Diffraction from the PKP caustic B. Bull. Seism. Soc. Am. **64**, 33–43, 1974

Červený, V., Ravindra, R.: Theory of seismic head waves. Toronto and Buffalo: Univ. of Toronto Press 1971

Chapman, C.H.: A first-motion alternative to geometrical ray theory. Geophys. Res. Letts., 1976

Choy, G.: Theoretical seismograms of core phases calculated by a frequency-dependent full wave theory, and their interpretation. To appear in Geophys. J. R. astr. Soc., 1977

Cormier, V.F., Richards, P.G.: Comments on 'The damping of core waves' by Anthony Qamar and Alfredo Eisenberg. J. Geophys. Res. **81**, 3066–3068, 1976

Cormier, V. F.: Ph. D. Thesis, Columbia University, New York, N. Y. 1976

Debye, P.J.: The electromagnetic field surrounding a cylinder and the theory of the rainbow. Phys. Z. **9**, 775–778, 1908

Doornbos, D.J.: Anelasticity of the inner core. Geophys. J. R. astr. Soc. **38**, 397–415, 1974

Dziewonski, A.M., Hales, A.L., Lapwood, E.R.: Parameterically simple earth models consistent with geophysical data. Phys. Earth Planet. Int. **10**, 12–48, 1975

Franz, W.: Theorie der Beugung elektromagnetischer Wellen. Berlin-New York: Springer 1957

Fuchs, K., Müller, G.: Computation of synthetic seismograms with the reflectivity method and comparison with observations. Geophys. J. R. astr. Soc. **23**, 417–433, 1971

Gilbert, F., Helmberger, D.V.: Generalized ray theory for a layered sphere. Geophys. J. R. astr. Soc. **27**, 57–80, 1972

Gilbert, F., Dziewonski, A.M.: An application of normal mode theory to the retrieval of structural parameters and source mechanisms from seismic spectra. Phil. Trans. R. Soc. Lond., Ser. A **278**, 187–269, 1975

Helmberger, D.V.: The crust-mantle transition in the Bering Sea. Bull. Seism. Soc. Am. **58**, 179–214, 1968

Hill, D.P.: Velocity gradients and anelasticity from crustal body wave amplitudes. J. Geophys. Res. **76**, 3309–3325, 1971

Julian, B.R., Anderson, D.L.: Travel times, apparent velocities and amplitudes of body waves. Bull. Seism. Soc. Am. **58**, 339–366, 1968

Kennett, B.L.N.: The effects of attenuation on seismograms. Bull. Seism. Soc. Am. **65**, 1643–1652, 1975

Langer, R.E.: The asymptotic solutions of ordinary linear differential equations to the second order, with special reference to a turning point. Trans. Am. Math. Soc. **67**, 461–490, 1949

Ludwig, D.: Diffraction by a circular cavity. J. Math. Phys. **11**, 1617–1629, 1970

Müller, G.: Amplitude studies of core phases. J. Geophys. Res. **78**, 3469–3490, 1973

Nussenzveig, H.M.: High-frequency scattering by a transparent sphere. I. Direct reflection and transmission. J. Math. Phys. **10**, 82–124, 1969

Phinney, R.A., Alexander, S.S.: *P* wave diffraction theory and the structure of the core-mantle boundary. J. Geophys. Res. **71**, 5959–5975, 1966

Rayleigh, Lord: The problem of the whispering gallery. Phil. Mag. **20**, 1001–1004, 1910

Richards, P.G.: Calculation of body waves for caustics and tunnelling in core phases. Geophys. J. R. astr. Soc. **35**, 243–264, 1973

Richards, P.G.: Weakly coupled potentials for high-frequency elastic waves in continuously stratified media. Bull. Seism. Soc. Am. **64**, 1575–1588, 1974

Richards, P.G.: On the adequacy of plane-wave reflection-transmission coefficients in the analysis of seismic body waves. Bull. Seism. Soc. Am. **66**, 701–718, 1976

Scholte, J.G.J.: On seismic waves in a spherical earth. Koninkl. Med. Meteorol. Inst. Publ. **65**, 1–55, 1956

Überall, H.: Surface waves in acoustics. In Physical acoustics, Vol. 10 (W. P. Mason, R. N. Thruston, eds.), pp. 1–60. New York: Academic Press 1975

Received November 8, 1976; Revised Version February 1, 1977